ISSN (Print) 1226-1750
ISSN (Online) 2233-6656
Journal of Magnetics 18(4), 473-480 (2013) http://dx.doi.org/10.4283/JMAG.2013.18.4.473

Durable and Sustainable Strap Type Electromagnetic Harvester for Tire Pressure Monitoring System

Soobum Lee[1] and Dong-Hun Kim[2]*

[1]*Department of Mechanical Engineering, University of Maryland Baltimore County, Baltimore, MD 21250, USA*
[2]*Department of Electrical Engineering, Kyungpook National University, Daegu 702-701, Korea*

(Received 8 September 2013, Received in final form 17 October 2013, Accepted 22 October 2013)

A new concept design of electromagnetic energy harvester is proposed for powering a tire pressure monitoring sensor (TPMS). The thin coil strap is attached on the circumferential surface of a rim and a permanent magnet is placed on the brake caliper system. When the wheel rotates, the relative motion between the magnet and the coil generates electrical energy by electromagnetic induction. The generated energy is stored in a storage unit (rechargeable battery, capacitor) and used for TPMS operation and wireless signal transmission. Innovative layered design of the strap is provided for maximizing energy generation. Finite Element Method (FEM) and experiment results on the proposed design are compared to validate the proposed design; further, the method for design improvement is discussed. The proposed design is excellent in terms of durability and sustainability because it utilizes the everlasting rotary motion throughout the vehicle life and does not require material deformation.

Keywords : electromagnetic induction, energy harvesting, finite element analysis, tire pressure monitoring sensor

1. Introduction

Tire pressure monitoring has been recognized as a key factor to increase fuel efficiency, avoid unnecessary tire wear, and more importantly, keep passengers safe. As a solution, a tire pressure monitoring system (TPMS) which is mounted inside the vehicle wheel to send the pressure signal wirelessly to the vehicle dashboard for real time pressure monitoring has been recently accepted. TPMS has been mandated on all new vehicles since 2007 in the U.S. [1] and 2012 in Europe [2]. TPMS is expected to become one of the most popular electronic products in vehicle applications, and the worldwide market volume is expected to exceed $3.0 billion by 2017 [3].

TPMS is usually composed of a pressure and temperature sensor, a RF transmitter and a power source. Chemical batteries, the widely used power source for TPMS, have several drawbacks, such as low durability and inferior sustainability [4] – batteries normally last for 7 to 10 years (less than 13 years or 200,000 km life of a vehicle), which are not sufficient, especially when vehicle makers are concerned with warranty costs [5]. Recently, there have been significant studies for an energy harvester [5, 6], which scavenges ambient energy and provides it to a TPMS, in order to overcome the limitations of battery lifetime and enable a maintenance-free TPMS.

Piezoelectric or electromagnetic conversion principles have been mainly considered to harvest the wasted energy from the vehicle wheel (e.g., vibration from wheel rotation, tire deformation) and store as electrical energy. For harvesting vibration energy, most harvesters have a spring-mass system of which the resonant frequency is tuned to the excitation frequency. Researches on cantilever type piezoelectric harvesters, one of the most actively studied designs, are well summarized in [7, 8] and multiple applications to TPMS are found in [9-11]. Mania *et al.* proposed an impact-based energy harvester using piezoelectric materials [12]. The embodied mass moves by centripetal force and impacts the piezoelectric transducer to generate 4 mW at 800 rpm wheel rotation speed. Recently, the piezoelectric nanowires are utilized to convert a piezoelectric potential from tire deformation to the output power density at around 70 $\mu W/cm^3$ [13]. Most of the electromagnetic harvesters with a cantilever beam are surveyed in [8, 14]. A relative motion by gravitational force between a stationary magnet and the coil attached to the rotating

*Corresponding author: Tel: +82-53-950-5603
Fax: +82-53-950-5603, e-mail: dh29kim@ee.knu.ac.kr

wheel enables energy generation for a TPMS [15, 16]. Theuss *et al.* proposed a coil embodied inside the tire where a voltage is induced with the magnetic fields around it [17]. Hatipoglu and Ürey implemented an electromagnetic energy harvester with a spiral FR4-made spring for broadband response frequency utilization to produce 40 μW with 15 m/s^2 acceleration input [18]. A similar type of energy harvester was proposed by Part *et al.* [19]. They performed the design optimization for the spiral spring shape to obtain low spring constant and a target natural frequency for low level ambient vibration harvesting. Wang *et al.* designed a well-weighted pendulum type harvester which adjusts its natural frequency to meet the wheel rotation frequency [20]. In-plane rotary electromagnetic generators with spiral coils connected in series are suggested by Holmes *et al.* [21], Pan and Wu [22] and Liao *et al.* [23]. Other researches on piezoelectric and electromagnetic harvesters can be found in [24].

Durability is always an issue for the piezoelectric harvester – piezoelectric ceramic material may easily fail due to its brittleness, especially when placed on the surface of the tire where high dynamic strain is observed. Even though a piezoelectric fiber or an elastomer-type material is used, the design for durability is still required because a piezoelectric harvester inherently requires material deformation. Electromagnetic harvesters are known to be one of the most robust energy conversion methods for utilizing the kinetic energy of vehicle wheels, particularly when the high temperature/pressure environment inside the tire is considered; the strength of neodymium magnet is stable under Curie temperature (more than 300 °C) [25] and the resistivity change of coil material (usually copper) is minor inside the tire environment [26].

To overcome the aforementioned drawbacks of previous energy harvesting devices, this paper proposes a new design concept of an electromagnetic energy harvester for TPMS. The proposed design does not require any material deformation or contact behavior; thus, the concern on mechanical failure is minimal. The details are explained in the main body of this paper which is organized as follows: the proposed conceptual design is explained in Section 2, the prototype and the numerical/experimental validation are included in Section 3, and the power evaluation with the discussion on design improvement is conducted in Section 4.

2. Proposed Design of Energy Harvester

The proposed energy harvesting device captures kinetic (rotational) energy and converts it into electrical energy

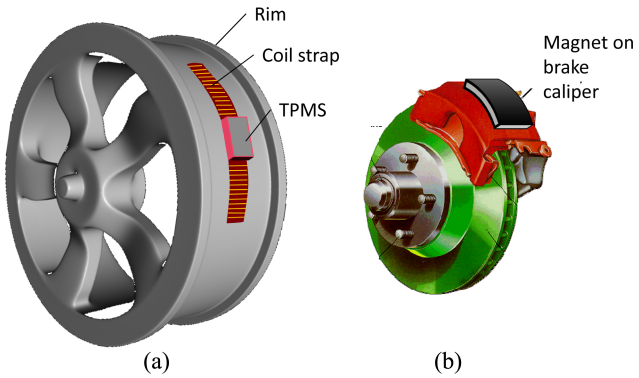

Fig. 1. (Color online) Prospective view of the proposed harvester assembled in a vehicle: (a) rim with coil strap, (b) brake caliper with magnet.

using electromagnetic induction through the coil strap attached inside the wheel rim [27]. The overall design concept is illustrated in Fig. 1. The rim is made of materials with very low conductivity/permeability in order (i) not to distort or weaken the magnetic fields to the coil and (ii) to minimize eddy current generation. A permanent magnet is placed on any stationary part around the wheel (e.g., brake caliper assembly). When the wheel rotates, relative motion occurs between the strap and the magnet. The electrical energy storage circuit is connected to the coil strap to save electrical energy in a storage device (e.g., supercapacitor or rechargeable battery). Finally, the saved energy is used to operate a TPMS module for pressure measurement and wireless transmission.

Fig. 2 displays the overall schematic of the proposed design. The cylindrical coordinate system shown in Fig. 2(a) has a z-axis, defined as the direction into the paper. On the outer surface of the brake caliper, the permanent magnet is attached so that the magnetic flux lines stretch along the θ-direction, as indicated with the dash dotted lines. The dashed line indicates the coil strap attached on

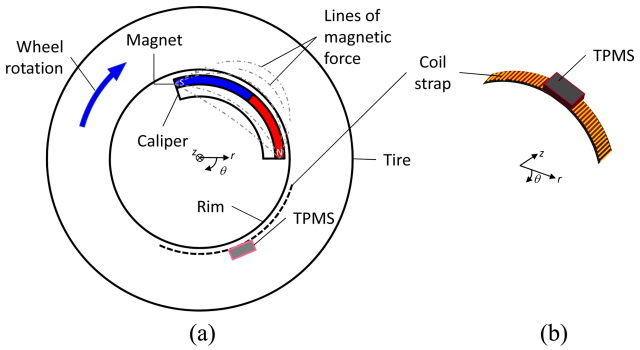

Fig. 2. (Color online) Design concept of the proposed harvester: (a) side view of main components, (b) coil strap.

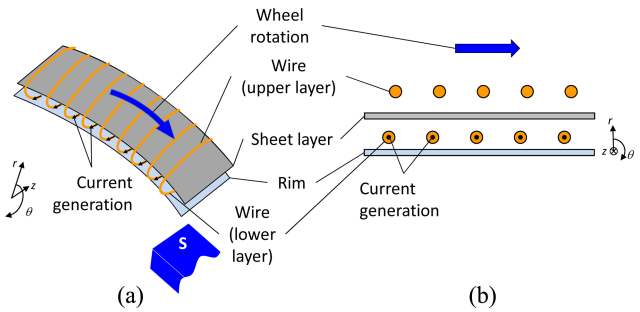

Fig. 3. (Color online) Coil strap with sheet layer: (a) perspective view (b) side view.

the surface of the rim. Fig. 2(b) shows the perspective view of the strap in which the coil wire is stretched along the z-direction. When the wheel rotates along the θ-direction, electrical current flows along the negative z-direction (out of the paper), according to Faraday's law of induction.

For the maximization of power generation, an innovative design of the coil strap, including ferromagnetic sheet layers, is provided. The details on the electromagnetic induction in the coil strap are explained in Fig. 3, where the strap approaches the south magnetic pole. Fig. 3(a) and (b) show a part of the strap in the perspective and side views, respectively. The coil strap consists of insulated wire and sheet layers; in addition, the coil is wound around the sheets.

The role of the magnetic sheet is explained in Fig. 4. The ferromagnetic sheet conducts magnetic flux lines better than air (and most other materials). In a sense, they capture the magnetic flux lines by providing a "path of least resistance," as shown on the right of Fig. 4 and accordingly, the linkage flux of the coil strap increases. It is known that aligning the sheet surface parallel (or nearly parallel) to the orientation of the magnetic flux lines will yield the least magnetic reluctance, as shown in Fig. 4 [28]. Consequently, the magnetic flux on the upper layer of the wire (Fig. 3(b)) is minimized. It is noted that magnetic flux lines perpendicular to the sheet will not change the path as they travel through the air, as shown on the left of Fig. 4.

When the wheel rotates, electrical current is generated along the negative z-direction in the lower part of the coil (below the sheet layer, indicated as "lower layer" in Fig. 3). Additional sheet layers can be added in the coil strap to reduce the reluctance of the magnetic system considered.

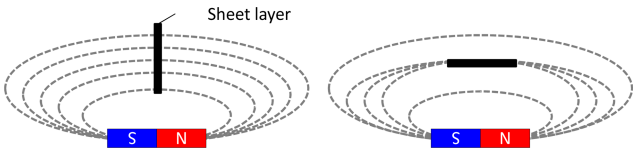

Fig. 4. (Color online) Effect of magnetic sheet core.

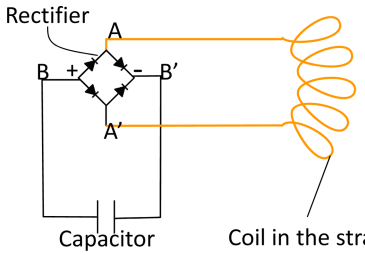

Fig. 5. (Color online) Circuit diagram with rectifier and capacitor.

The voltage from the wire is rectified so that the AC voltage signal is converted to DC voltage. Fig. 5 is the arrangement for a charging circuit composed of a rectifier and a capacitor in which the harvested energy is accumulated.

3. Prototype Fabrication and Analysis on Voltage Generation

3.1. Prototype fabrication

The concept design of the harvester in Section 2 is prototyped. To analyze and validate its performance, both numerical and experimental methods are carried out. The specification for the magnet and materials used are listed in Table 1.

The experimental setup utilizing a bicycle is chosen to simulate a vehicle wheel rotation, as shown in Fig. 6. For easy measurement, the coil strap is placed on a stationary position (e.g., bicycle frame) and the magnet is attached on the rim. The gap between the magnet and the coil strap is about 1 in (2.54 cm). A stainless steel plate (3.5 mm thick) is placed between the coil and the wheel to investigate the eddy current effect in the rim material. The harvester prototype (coil strap) is shown in Fig. 7. Cardboard box papers are used for the intermediate nonconductive layers. Relatively, thick papers are chosen for easy insertion and subtraction of the sheet layers by hand so that the effect of the sheet layers can be easily examined. In a real implementation, a compactly designed coil strap will be attached on a vehicle rim, as explained in Section 2. The capacitance in Fig. 5 is chosen as 1,000 μF.

3.2. Waveform Analysis

To record the output signal, the data acquisition board (NI DAQCard-6024E [29]) with NI BNC-2120 connector [30] and LabView 8.0 is used. Fig. 8 shows the waveform of open circuit voltage (V_{oc}), which is measured at terminal

Table 1. Material specification for the generator.

Part	Subpart	Item	Value
	Neodymium magnet	Size	$10.16 \times 2.54 \times 1.27$ cm^3
		Surface magnetic field	3424 G
Coil	Wire	Diameter	0.255 mm (30 AWG)
		Length	60.96 m (around 800 turns)
		Material	Copper w/enamel coating
	Sheet layer	Magnetic saturation	21400 G
		Maximum permeability	4000
		Thickness	0.254 mm
	Intermediate nonconductive layer	Material	Cardboard box paper
		Thickness	3 mm

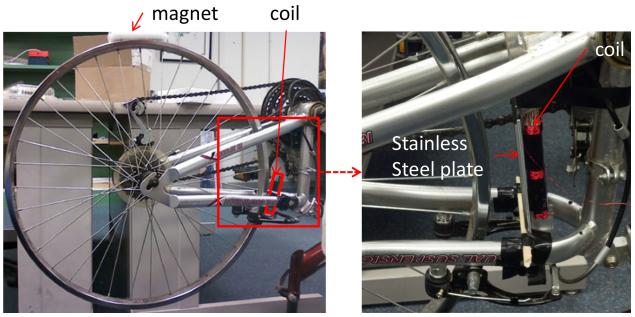

Fig. 6. (Color online) Experiment setup with bicycle.

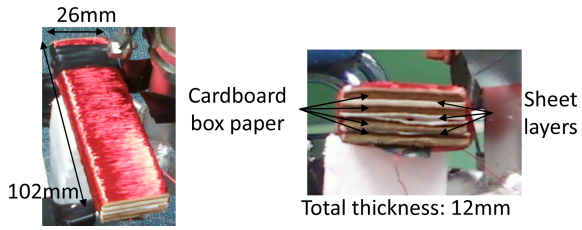

Fig. 7. (Color online) Coil strap with variable number for sheet cores.

A-A' in Fig. 5 (without rectifier), when the wheel rotates at 24.9 km/h (or 200 rpm) and three sheet layers are used.

The waveform can be divided into three phases, as shown in Fig. 8, as the magnet passes the coil strap. According to Faraday's law, the induced voltage is proportional to the time rate of linkage flux of the coil strap ($\partial\lambda/\partial\tau$). When the south pole approaches (Phase I in Fig.

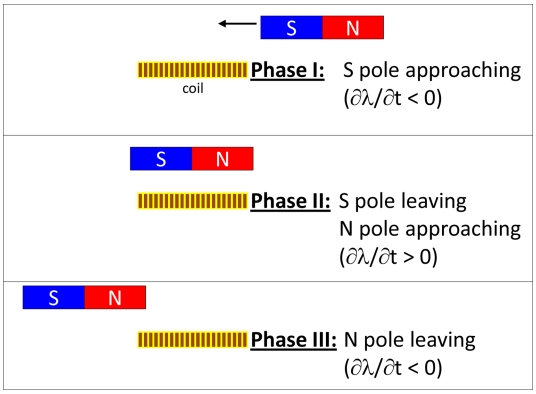

Fig. 9. (Color online) Waveform analysis.

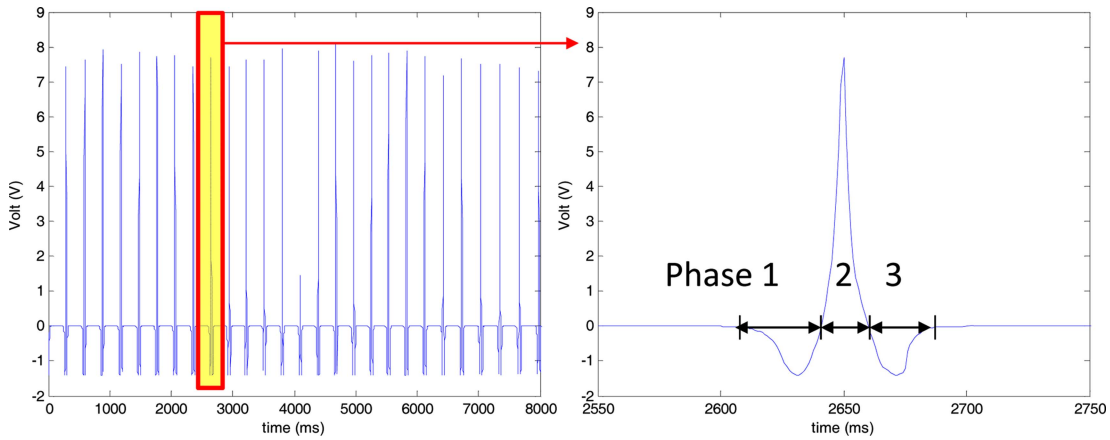

Fig. 8. (Color online) Waveform of V_{oc}.

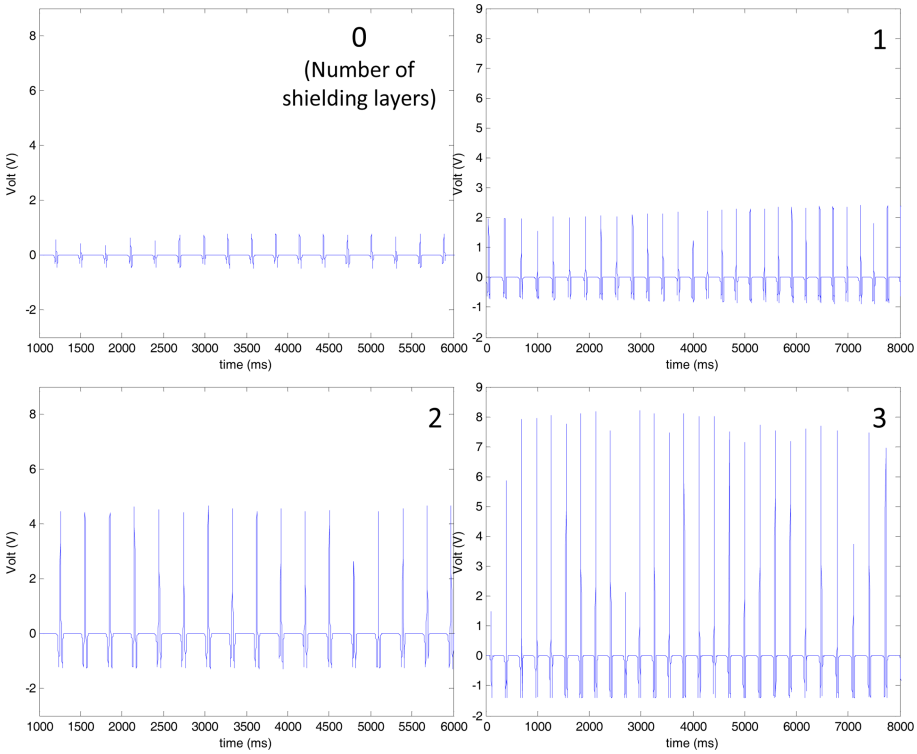

Fig. 10. (Color online) Waveform of V_{oc} with different number of sheet layers.

9), $\partial\lambda/\partial\tau < 0$, it produces negative voltage. In Phase II, where $\partial\lambda/\partial\tau$ becomes positive, the positive voltage is generated because the south pole leaves and the north pole approaches. In the case of Phase III, the north pole leaves and $\partial\lambda/\partial\tau$ becomes negative in order to generate the negative voltage.

3.3. Study on the sheet layer effect

The effect of the magnetic sheet core (shielding layer) is thoroughly examined in this section. The number of the layers is changed from 0 to 3; further, it also tests the two rotating speeds of 97 and 200 rpm (12.1 and 24.9 km/h). The experimental results are obtained, as in Fig. 10, which shows larger V_{oc} amplitude with the increased number of layers.

The test has been performed repeatedly and the peak value of V_{oc} has been observed, as shown in Table 2 and Fig. 11, which show the monotonic increase of V_{oc} as the number of sheet layers increases. When a cubic polynomial curve fitting is attempted for the data presented in Table 2,

$$V_{oc} = -0.045x^3 + 0.414x^2 + 0.326x + 0.377 \quad (1)$$

for the low speed (SSE, sum of square error = 2.28×10^{-30}) and

Table 2. Open circuit voltage measurement and FEM analysis.

	Number of layers	0	1	2	3
Low speed[a] (12.1 km/h)	Mean (V_{oc})	0.38	1.07	2.33	3.87
	Standard deviation (V_{oc})	0.02	0.05	0.17	0.47
	Number of peaks	75	75	81	78
	FEM (V_{oc})	0.32	0.98	2.09	3.45
High speed[b] (24.9 km/h)	Mean (V_{oc})	0.73	2.08	4.35	7.35
	Standard deviation (V_{oc})	0.08	0.24	0.69	1.15
	Number of peaks	158	113	150	158
	FEM (V_{oc})	0.63	1.95	4.17	6.90

[a]97 rpm
[b]200 rpm

$$V_{oc} = -0.031x^3 + 0.554x^2 + 0.829x + 0.731 \quad (2)$$

for the high speed (SSE = 1.59×10^{-30}), where x is the number of sheet layers. In both cases, strong quadratic behaviors are observed (V_{oc} increases in a quadratic order as the number of layers increases). However, it can be assumed that the effect of the sheet layers will be saturated if a larger number of sheets is attempted, which remains as future work.

To investigate the layer effect, a three-dimensional finite element model of the prototype is constructed in Fig. 12. While taking into account the nonlinear property of the

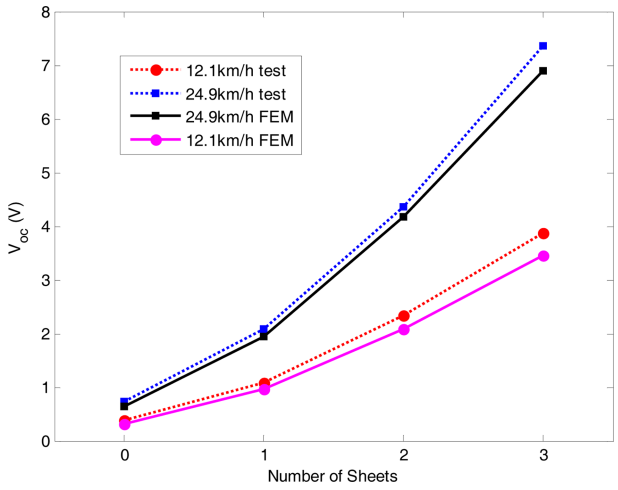

Fig. 11. (Color online) Effect of the number of sheet layers to V_{oc}.

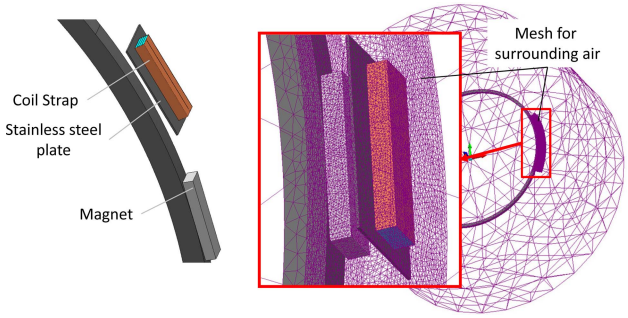

Fig. 12. (Color online) Finite element model of the prototype TPMS.

sheet layer, 753,991 tetrahedral elements are used with the second-order interpolation function. For obtaining reliable numerical solutions, a general-purpose analysis tool, called MagNet VII, is utilized. As shown in Fig. 13, the sheet layer plays a role in strengthen the linkage flux between the magnet and the coil strap by providing the path of least resistance. Table 2 and Fig. 11 also show the simulation results, which have excellent agreement with the experiment.

The effect of stainless steel plate is studied, as demonstrated in Table 3. The test results show no significant effect on the existence/nonexistence of the stainless plate, which is found because of the relatively low conductivity (7.20×10^{-7} Wm, 20 °C) and low magnetic susceptibility

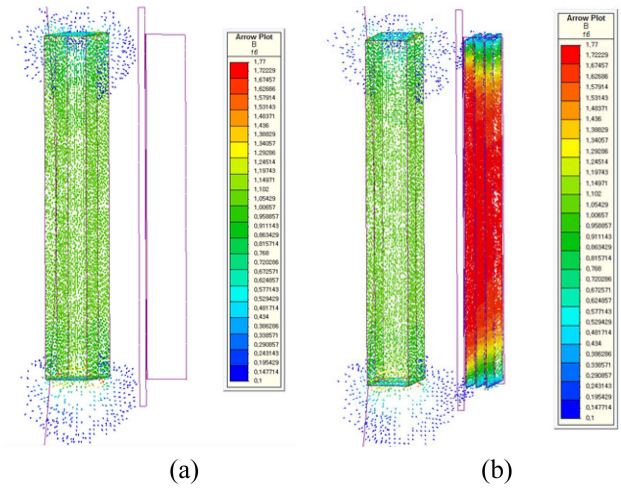

Fig. 13. (Color online) Arrow plots of magnetic flux density: (a) air core, (b) three-sheet core.

($9.2\sim13.3 \times 10^{-5}$); moreover, the generation of the eddy current was minimal.

4. Power Evaluation

V_{oc} generated from the proposed harvester does not show a sinusoidal waveform. Thus, it is difficult to evaluate the expected power analytically. The power can be experimentally measured with a simple charging circuit, as shown in Fig. 5. The accumulated voltage in the capacitor is measured multiple times under the wheel speed at 24.9 km/h (200 rpm). The charging curve, shown in Fig. 14, is composed of three parts: without capacitor (before charging), charging with capacitor and discharging after the rotation stops. Once the capacitor is connected, the voltage increases and is saturated at around 4 to 4.5 V. Once the human input is stopped through the crankshaft (around 12 seconds, as indicated by the arrow in the figure), the wheel speed reduces and it slightly lowers the voltage peak frequency and amplitude, simultaneously. Once the wheel is enforcedly stopped, the voltage starts being discharged from the capacitor.

The time-average power is calculated as

$$P = \frac{1}{T}\int V(t)I(t)dt\,, \tag{3}$$

Table 3. Rim material effect on open circuit voltage.

Maximum open circuit voltage (V_{oc})	With rim material		Without rim material	
	Mean	Standard deviation	Mean	Standard deviation
Low speed (8 km/h)	2.450	0.121	2.401	0.089
High speed (21 km/h)	6.506	0.074	6.299	0.176

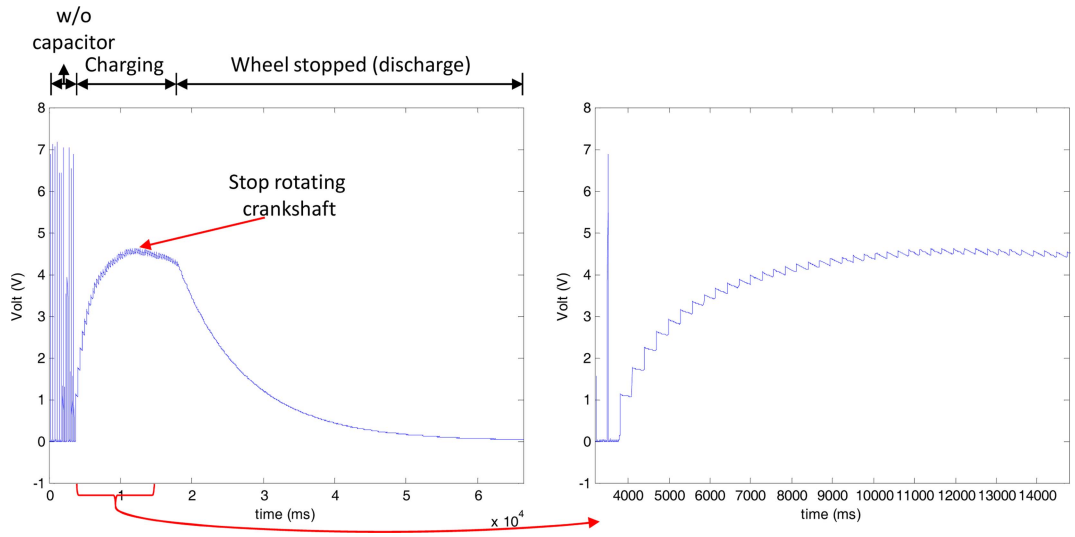

Fig. 14. (Color online) Charging/discharging curve.

Table 4. Power measurement.

Trial	Power (mW)
1	3.0
2	3.0
3	3.1
4	3.1
5	3.0
6	3.0
Mean	3.05

where T is the charging time, and $V(t)$ and $I(t)$ mean the instantaneous capacitor voltage and current values, respectively. The charging experiments have been carried out 6 times, as shown in Table 4, where a 1,000 μF capacitor was used. The experimental result consistently yields almost the same average power amount of 3.0 mW.

4.1. Discussion

A state-of-the-art TPMS module requires about 200-250 μW for RF data transmission with a length of 100 bit and a transmission rate of 10 Kbit/sec; however, the average power consumption for each datagram can be reduced to 10-15 μW, particularly by reducing the power-down current [6]. Thus, the experimental and numerical study found that the current prototype sufficiently generates the required power for TPMS. In a real implementation, however, the following design factors should be considered in order to achieve design compactness while maintaining power requirement. First, the strength of the magnetic field will be affected by the choice of the magnet and the gap between the magnet and coil. The magnet should be chosen not to cause any malfunction of electronic systems in a vehicle, and the gap must be determined to prevent any possible structural interference between the brake caliper and the wheel. Second, an improved coil winding method or resizing/reshaping the strap needs to be considered in order to enlarge the coil fill factor. Third, appropriate choice on the rim materials is required in order to have excellent mechanical properties with low conductivity and low magnetic property. Stainless steel or titanium can be an appropriate choice due to their relatively low conductivity (high resistivity) and low magnetic susceptibility, as proven in Session 3.3. New composite rim material development is under way [29, 30], which will enable successful commercialization of the proposed design with no concerns on the eddy current issue.

5. Conclusion

A thin strap type energy harvester is proposed in this paper for powering a tire pressure monitoring sensor (TPMS). The unique design of the coil strap with the sheet layer enables a sufficient voltage generation–power at about 3.0 mW is generated with three sheet layers when the wheel rotates at 200 rpm (or 24.9 km/h), and larger power generation is expected with more sheet layers and faster rotating speed.

The innovative design significantly enhances durability because the proposed design does not require material deformation or wear. Design improvement for the compactness of the proposed harvester is still required. Additional verification study with an automobile under the variable rotating speed will be performed to ensure sustainable power generation and excellent durability. In order to ensure durability, possible design modification can be

made by including the shock absorbing layer (between the rim and the harvester, or between the magnet and the caliper).

Acknowledgment

The authors thank Dr. D. K. Kwon and Dr. A. Kareem (NatHaz Laboratory, CEGS, University of Notre Dame) for providing support with the data acquisition board and some necessary equipment.

References

[1] US DOT National Highway Traffic Safety Administration. Federal motor vehicle safety standards; tire pressure monitoring systems; controls and displays (2005); Available from: http://www.nhtsa.gov/cars/rules/rulings/tpms-finalrule.6/tpmsfinalrule.6.html
[2] European Commission Enterprise and Industry. Paving the way for safer and greener cars, Enterprise & Industry Online Magazine (2008); Available from: http://ec.europa.eu/enterprise/magazine/articles/better-regulation/article_7009_en.htm
[3] Global Industry Analysts Inc. Tire pressure monitoring systems (TPMS) - a global strategic business report (2011); Available from: http://www.strategyr.com/Tire_Pressure_Monitoring _Systems_TPMS_Market_Report.asp
[4] Wikipedia. Tire-pressure monitoring system (2011); Available from: http://en.wikipedia.org/wiki/Tire-pressure_monitoring_system
[5] PowerMEMS, S. Roundy, Proc. (2008) pp 1-6.
[6] M. Lohndorf, T. Kvister, E. Westby, and E. Halvorsen, Proc. Power MEMS, Nov. 28-29, Freiburg, Germany (2007) pp 331-334.
[7] A. Erturk and D. J. Inman, Piezoelectric Energy Harvesting, Wiley (2011).
[8] S. Priya and D. J. Inman, Energy Harvesting Technologies, Springer Verlag (2008).
[9] D. V. Nowicki and C. A. Munroe, US Patent 5945908 (1999).
[10] L. Pinna, M. Valle, and G. M. Bo, Proc. 3th Italian Conf. Sens. Microsyst. (2009) pp 450-455.
[11] Q. Zheng, H. Tu, A. Agee, and Y. Xu, Proc. Power-MEMS (2009) pp 403-406.
[12] G. Manla, N. M. White, and J. Tudor, Proc. Transducers, June 21-25, Denver, CO, USA (2009) pp 1389-1392.
[13] Y. Hu, C. Xu, Y. Zhang, L. Lin, R. L. Snyder, and Z. L. Wang, Adv. Mater. **23**, 4068 (2011).
[14] T. Kazmierski, Energy Harvesting Systems: Principles, Modeling and Applications, Springer Verlag (2010).
[15] S. B. DiMauro and A. C. Lesesky, US Patent 8405235 B2 (2010).
[16] J.-H. Huang, US Patent 20100156618 A1 (2009).
[17] H. Theuss and K. Elian, US Patent 20090256361 A1 (2008).
[18] G. Hatipoglu and H. Ürey, Smart Mater. Struct. **19**, 015022 (2010).
[19] J. C. Park, D. H. Bang, and J. Y. Park, IEEE Trans. Magn. **46**, 1937 (2010).
[20] Y. J. Wang, C. D. Chen, and C. K. Sung, Sens. Actuators: A **159**, 196 (2010).
[21] A. S. Holmes, G. Hong, and K. R. Pullen, J. Microelectromech. S. **14**, 54 (2005).
[22] C. T. Pan and T. T. Wu, Journal of J. Micromech. Microeng. **17**, 120 (2007).
[23] L. D. Liao, P. C. P. Chao, J. T. Chen, W. D. Chen, W. H. Hsu, and C. W. Chiu, Magnetics, IEEE Trans. Magn. **45**, 4621 (2009).
[24] A. Khaligh, P. Zeng, and C. Zheng, IEEE Trans. Ind. Electron. **57**, 850 (2010).
[25] Wikipedia. Neodymium magnet (2011); Available from: http://en.wikipedia.org/wiki/Neodymium_magnet
[26] Wikipedia. Electrical resistivity and conductivity (2011); Available from: http://en.wikipedia.org/wiki/Electrical_resistivity_and_conductivity
[27] S. Lee, Korea Patent KR/10-1310461, 2013.
[28] Less EMF. Guidelines for installing magnetic shielding (2011); Available from: http://www.lessemf.com/guidelines.pdf
[29] S. Yuan and K. P. Maurer, US Patent 20120001476 A1 (2012).
[30] J. D. D. Silva and M. Tiraboschi, US Patent 20120146395 (2012).